



HAL
open science

Crystalline tetrazepam as a case study on the volume change on melting of molecular organic compounds

Ivo Rietveld, Philippe Négrier, Maria Barrio, Hassan Allouchi, René Ceolin, Josep-Lluís Tamarit

► To cite this version:

Ivo Rietveld, Philippe Négrier, Maria Barrio, Hassan Allouchi, René Ceolin, et al.. Crystalline tetrazepam as a case study on the volume change on melting of molecular organic compounds. International Journal of Pharmaceutics, 2020, 593, pp.120124. 10.1016/j.ijpharm.2020.120124 . hal-03053325

HAL Id: hal-03053325

<https://normandie-univ.hal.science/hal-03053325>

Submitted on 15 Dec 2022

HAL is a multi-disciplinary open access archive for the deposit and dissemination of scientific research documents, whether they are published or not. The documents may come from teaching and research institutions in France or abroad, or from public or private research centers.

L'archive ouverte pluridisciplinaire **HAL**, est destinée au dépôt et à la diffusion de documents scientifiques de niveau recherche, publiés ou non, émanant des établissements d'enseignement et de recherche français ou étrangers, des laboratoires publics ou privés.



Distributed under a Creative Commons Attribution - NonCommercial 4.0 International License

CRYSTALLINE TETRAZEPAM AS A CASE STUDY ON THE VOLUME CHANGE ON MELTING OF MOLECULAR ORGANIC COMPOUNDS

Ivo B. Rietveld^{1,2*}, Philippe Negrier³, Maria Barrio⁴, Hassan Allouchi⁵, René Ceolin⁴, Josep-Lluís Tamarit^{4*}

¹ SMS Laboratory (EA 3233), Université de Rouen-Normandie, Place Émile Blondel, Mont Saint Aignan 76821, France

² Faculté de Pharmacie, Université Paris Descartes, USPC, 4 avenue de l'observatoire, 75006, Paris, France

³ LOMA, UMR 5798, CNRS, Université de Bordeaux, F-33400 Talence, France

⁴ Grup de Caracterització de Materials, Departament de Física and Barcelona Research Center in Multiscale Science and Engineering Universitat Politècnica de Catalunya, EEBE, Campus Diagonal-Besòs, Av. Eduard Maristany 10-14, 08019 Barcelona, Catalonia, Spain.

⁵ EA 7502 SIMBA, Synthèse et Isolement de Molécules BioActives, Laboratoire de Chimie Physique, Faculté de Pharmacie, 31, Avenue Monge, 37200 Tours, France

* Corresponding authors : ivo.rietveld@univ-rouen.fr, josep.lluis.tamarit@upc.edu

20 ABSTRACT

21 The volume change on melting is a rarely studied quantity and it is not well understood even if it must
22 reflect the changes in interaction between the solid and the liquid state. It is part of the solid-state
23 information for materials and pharmaceuticals and it is important for the reliability of polymorph stability
24 study results. Using the crystal structure of monoclinic tetrazepam at 150 K and at room temperature, in
25 addition to powder X-ray diffraction as a function of the temperature, the specific volume of tetrazepam
26 has been determined over a large temperature domain. In combination with a pressure-temperature
27 curve for the melting of tetrazepam, its volume change on melting could be determined. With this
28 information and previous data from the literature, the assumption that the volume of the solid increases
29 on average with 11% on melting has been investigated. It can be concluded that this value is not constant;
30 however so far, no simple relationship has been found to relate the solid state to its volume change on
31 melting and using 11% remains best practice. A comparison of the tetrazepam crystal structure with
32 diazepam and nordiazepam has been provided too.

33

34 Keywords:

35 Crystal structure; specific volume; calorimetry; phase behavior; phase diagram; X-ray diffraction;
36 molecular interaction

37

38 1 INTRODUCTION

39 Once an active pharmaceutical ingredient (API) has been synthesized, in addition to the toxicological and
40 activity measurements, a preliminary physical characterization is carried out too. The latter is important
41 because once the molecule is considered to be viable API, it will need to be formulated in the most
42 appropriate way. Although the formulation may ideally depend on the activity and patient requirements,
43 unfortunately often the physical behavior has its demands too. The properties of the solid form such as
44 salts, co-crystals, or hydrates and polymorphism may lead to a number of difficult questions to answer or
45 to unexpected problems even if the formulation itself is liquid-based (Bauer et al., 2001; Céolin and
46 Rietveld, 2015; Chaudhuri, 2008; Rietveld and Ceolin, 2015). It is obvious that from an industrial point of
47 view, quick answers with as little as possible experimental effort are preferred, as long as the answers can
48 be trusted. In addition, it may be that certain measurements cannot be carried out due to decomposition
49 or the absence of sufficient API in the early stages of development, when choices nonetheless will have to
50 be made about formulation that could affect 2nd and 3rd phase results due to bioavailability.

51 It is nowadays customary to carry out experimental and in-silico polymorph screening. However, once the
52 existing polymorphs (i.e. the experimentally verified polymorphs) have been determined, it is not always
53 easy to determine the stability ranking of the polymorphs and the conditions at which the ranking applies.
54 It is for this reason that the method for constructing topological pressure-temperature phase diagrams
55 has been developed (Ledru et al., 2007; Toscani et al., 2002). This method can be used to obtain a full map
56 of the stability ranking between polymorphs over the entire temperature and pressure domain. With such
57 a phase diagram, it will be easy to judge whether an API may be sensitive to compression in tableting for
58 example or on heating during manufacturing or also storage. Such topological phase diagrams, that mainly
59 consist of extrapolations obtained through standard laboratory experiments such as differential scanning
60 calorimetry and X-ray diffraction, can guide decisions whether temperature or pressure should be further
61 explored or that one polymorph can be safely considered the most stable one.

62 To ensure that the topological phase diagrams are as trustworthy as they can be, it is important that they
63 are based on as many pertinent experimental data as possible. In that way, statistics and the outliers will
64 help discerning the boundaries of applicability of the topological method. Hence, this paper explores the
65 statistics of the volume change on melting of APIs, one of the quantities that is frequently used in the

66 construction of topological phase diagrams. The volume change between a solid polymorph and the liquid,
67 $\Delta_{\text{fus}}V$, at ordinary pressure is necessary to calculate the slope of the melting curve in the pressure-
68 temperature phase diagram. The slope is given by the Clapeyron equation:

$$69 \quad dP/dT_{\text{fus}} = \Delta_{\text{fus}}S/\Delta_{\text{fus}}V = \Delta_{\text{fus}}H/(T_{\text{fus}} \Delta_{\text{fus}}V) \quad (1),$$

70 where $\Delta_{\text{fus}}H$ and $\Delta_{\text{fus}}V$ are the enthalpy and volume changes, respectively, on melting at the melting
71 temperature T_{fus} .

72 However, while the melting temperature and enthalpy change of fusion can be obtained easily by
73 differential scanning calorimetry, the volume change $\Delta_{\text{fus}}V$ is by contrast almost never measured. It can be
74 done by measuring the densities of the solid and the liquid as a function of the temperature; however, this
75 is seldom carried out, because thermal degradation occurs frequently (in particular for drug substances),
76 while the sample is kept in the molten state, thus preventing the specific volume of the melt from being
77 correctly determined (Allouchi et al., 2014; Barrio et al., 2012; Brown and Glass, 2003; Henriët et al., 2016;
78 Huang et al., 2017; Mahé et al., 2013; Rietveld et al., 2018; Tetko et al., 2014; Valentini et al., 2018).

79 When density measurements of the liquid cannot be performed, a possible way to acquire additional data
80 consists of measuring the temperature and enthalpy of fusion of the solid in question in combination with
81 the pressure-temperature melting curve. Using the Clapeyron equation (eq. 1) the volume change on
82 melting at the melting temperature and at normal pressure can then be obtained. After adding this value
83 to the specific volume of the solid at T_{fus} and at normal pressure, which can be obtained from the thermal
84 expansion of the solid, the specific volume of the liquid at T_{fus} is obtained. This allows the calculation of the
85 ratio $v_{\text{liquid}}/v_{\text{solid}}$ at T_{fus} and at normal pressure.

86 Previous determinations indicate that the volume change on melting for most APIs and other small
87 organic molecules is such that the ratio $v_{\text{liquid}}/v_{\text{solid}}$ is about 1.10-1.12, *i.e.* a value that can tentatively be
88 considered to be almost constant irrespective of the organic molecular solid (Barrio et al., 2017; Céolin
89 and Rietveld, 2015; Goodman et al., 2004). Nevertheless, this experimental observation needs more
90 support by a larger number of experimental values. The question of whether the ratio is constant remains
91 therefore open, as will be discussed in this paper together with the predictive character of the
92 abovementioned ratio.

93 In the present paper, the solid state of monoclinic tetrazepam (inset in Figure 1), an active pharmaceutical
94 ingredient with muscle relaxant properties is presented. A comparison of its crystal structure with that of
95 the similar molecules, diazepam and nordiazepam, is provided. Finally, making use of the specific volume
96 obtained as a function of the temperature by powder diffraction, the volume difference between the solid
97 and liquid on melting has been determined and the statistics on this quantity have been discussed.

98 2 EXPERIMENTAL

99 2.1 SAMPLES

100 Single crystals of tetrazepam, whose crystal structure was solved previously at 293 K (Allouchi et al.,
101 2019), were obtained by slowly evaporating solutions in methanol at room temperature using a powder of
102 medicinal grade kindly supplied by Daiichi Sankyo France SAS. Since the X-ray diffraction profile of the
103 commercial sample was the same as the calculated one from the crystal structure, the powder was used as
104 such, and the crystal structure was redetermined at 150 K.

105 2.2 SINGLE CRYSTAL X-RAY DIFFRACTION

106 X-ray diffraction intensities were collected at 150 K on an Xcalibur-2 diffractometer with Sapphir-2 CCD
107 area detector and monochromatized Mo-K α radiation (0.71073 Å). The collection method involved ω -
108 scans having a width of 1°. The data collection, unit-cell refinement, and data reduction were performed
109 using the CrysAlis Pro, Oxford Diffraction Ltd. software package (Agilent-Technologies, 2014). Analytical
110 numeric absorption correction was carried out using a multifaceted crystal model (Clark and Reid, 1995).
111 The positions of non-H atoms were determined and refined by the SHELXS program (Sheldrick, 2008).
112 Non-hydrogen atoms were first refined isotropically followed by anisotropic refinement by full matrix
113 least-squares calculations based on F^2 using SHELXe (Hubschle et al., 2011). The positions of the H-atoms
114 were deduced from coordinates of the non-H atoms and Fourier synthesis. H-atoms were included for
115 structure factor calculations but not refined. Publication materials were generated using WinGX (Farrugia,
116 2012) and Mercury-3.3 (Macrae et al., 2008).

117

118 2.3 HIGH-RESOLUTION X-RAY POWDER DIFFRACTION (HR-XRPD)

119 XRPD measurements were performed with a vertically mounted INEL cylindrical position-sensitive
120 detector (CPS-120) using the Debye–Scherrer geometry and transmission mode. Monochromatic Cu-K α_1
121 ($\lambda = 1.54056 \text{ \AA}$) radiation was selected by means of an asymmetrically focusing incident-beam curved
122 quartz monochromator. Measurements as a function of temperature were performed using a liquid
123 nitrogen 700 series Cryostream Cooler from Oxford Cryosystems. Cubic phase Na₂Ca₃Al₂F₄ was used for
124 external calibration. PEAKOC application from DIFFRACTINEL software was used for the calibration as
125 well as for the peak position determinations after pseudo-Voigt fittings and lattice parameters were
126 refined by way of the least-squares option of the FullProf suite (Rodriguez-Carvajal, 1993; Rodriguez-
127 Carvajal et al., 2005).

128 Specimens were introduced in a Lindemann capillary (0.5-mm diameter) and allowed to rotate
129 perpendicularly to the X-ray beam during the experiments to improve the averaging of the crystallite
130 orientations. Before each isothermal data acquisition, the specimen was allowed to equilibrate for about
131 10 min, and each acquisition time was at least 1 h. The heating rate in between data collection was 1.33 K
132 min⁻¹. The diffraction patterns of tetrazepam, diazepam, and nordiazepam have been recorded as a
133 function of the temperature from about 100 K up to their respective melting points.

134 2.4 DIFFERENTIAL SCANNING CALORIMETRY (DSC)

135 Temperature (onset) and heat of fusion were obtained with a Q100 thermal analyzer from TA Instruments
136 at heating rates from 2 to 10 K min⁻¹. The analyzer was calibrated by using the melting point of indium
137 ($T_{\text{fus}} = 429.75 \text{ K}$ and $\Delta_{\text{fus}}H = 3.267 \text{ kJ mol}^{-1}$). The specimens were weighed using a microbalance sensitive to
138 0.01 mg and sealed in aluminum pans.

139 2.5 HIGH-PRESSURE DIFFERENTIAL THERMAL ANALYSIS (HP-DTA)

140 HP-DTA measurements have been carried out at 2 K min⁻¹ using a home-made high-pressure differential
141 thermal analyzer similar to Würflinger's apparatus and operating in the 298 – 473 K and 0 – 250 MPa
142 ranges (Würflinger, 1975). To determine the melting temperature as a function of pressure and to
143 ascertain that in-pan volumes were free from residual air, specimens were mixed with an inert
144 perfluorinated liquid (Galden®, from Bioblock Scientifics, Illkirch, France) as a pressure-transmitting

145 medium, and the mixtures were sealed into cylindrical tin pans. To check that the perfluorinated liquid
146 was chemically inactive and should thus have no influence on the melting temperature of tetrazepam,
147 preliminary DSC measurements were carried out with a Galden®-tetrazepam mixture on a Q100 analyzer
148 of TA instruments without applied pressure.

149 3 RESULTS

150 3.1 THE CRYSTAL STRUCTURE AT 150 K

151 The crystal structure at 150 K was found to be the same monoclinic $P2_1/c$ structure ($Z = 4$) as the one
152 solved at 293 K (Allouchi et al., 2019). Structural information can be found in the Supplementary
153 Materials: Crystal and structure refinement data (Table S1), atom labels (Figure S2), fractional
154 coordinates, bond lengths, bond angles, anisotropic displacement parameters, torsion angles and
155 hydrogen bonds (Tables S2 to S6, respectively). The Cambridge Crystallographic Data Centre (CCDC)
156 deposit number 2025809 contains the supplementary crystallographic data for this paper. It can be
157 obtained free of charge from the CCDC via www.ccdc.cam.ac.uk/data_request/cif.

158 Lattice parameters at 150 K were found to be: $a = 12.5260(2) \text{ \AA}$, $b = 11.2860(2) \text{ \AA}$, $c = 10.2714(2) \text{ \AA}$, $\beta =$
159 $102.378(2)^\circ$, $V_{\text{cell}} = 1418.30(4) \text{ \AA}^3$, leading to a density ($Z = 4$) of $1.35232(6) \text{ g cm}^{-3}$ and a specific volume of
160 $v = 0.73947(4) \text{ cm}^3 \text{ g}^{-1}$.

161 3.2 THE SPECIFIC VOLUME OF TETRAZEPAM AS A FUNCTION OF THE TEMPERATURE

162 Lattice parameters as a function of the temperature have been determined by X-ray powder diffraction
163 measurements between about 150 K and the melting point for tetrazepam, diazepam, and nordiazepam.
164 The corresponding specific volumes of tetrazepam as a function of the temperature are presented in
165 Figure 1. Values of lattice parameters and specific volumes have been compiled in Table S7. Thermal
166 expansion data for diazepam and nordiazepam can be found in Tables S8 and S9.

167 The values of the specific volume have been fitted to the linear equation:

$$168 \quad v/\text{cm}^3 \text{ g}^{-1} = 0.7169(10) + 1.46(3) \cdot 10^{-4} T/\text{K} \quad (R^2 = 0.996) \quad (2)$$

169 The specific volumes from the single crystal data at 293 K (Allouchi et al., 2019) and at 150 K are in close
170 agreement with those obtained by X-ray powder diffraction (Figure 1).

171 3.3 CALORIMETRIC BEHAVIOR

172 Calorimetric measurements under normal pressure have been carried out for several samples using
173 heating rates ranging from 2 to 10 K min⁻¹. The results have been compiled in Table S10 in the
174 Supplementary Materials. On heating from room temperature (curve 1 in Figure 2), a single endothermic
175 peak ascribed to the melting of tetrazepam was measured with an onset at $T_{\text{fus}} = 415.6(1.2)$ K and an
176 enthalpy change of 88.6(4.6) J g⁻¹ (25.6(1.3) kJ mol⁻¹). Upon cooling the melt down to 200 K, no
177 recrystallization-related thermal event was observed.

178 On reheating, after cooling the melt down to 200 K, a glass transition (midpoint at 315.0(1.0) K) was
179 observed (curve 2 and inset in Figure 2) followed by the recrystallization of the metastable melt and,
180 finally, by the melting of the monoclinic form. It is worth mentioning that the melting process
181 corresponding to samples previously melted takes place at a slightly lower temperature and, for heating
182 rates higher than 5 K·min⁻¹ with a smaller enthalpy change. The first experimental fact is associated with a
183 possible decomposition in the liquid state, while the second fact is due to a partial recrystallization
184 because the exothermic process involves also a smaller enthalpy change.

185 3.4 THERMAL BEHAVIOR UNDER PRESSURE

186 The temperature of fusion (onset) has been determined at various pressures ranging from 0 to 200 MPa
187 (see Figure 3b) and the pressure-temperature phase diagram has been constructed and is provided in
188 Figure 3a. The values have been compiled in Table S11 of the Supplementary Materials. A slight curvature
189 visible in the experimental solid-liquid equilibrium curve (dashed line as a guide for the eye in Figure 3a)
190 indicates that the pressure dependence of the melting temperature is slightly non-linear, which is caused
191 by the difference in the response to the pressure by the solid and the liquid.

192 Despite the slight curvature, the data can be fitted with a linear function with reasonable accuracy due to
193 the narrow pressure range:

$$194 \quad T_{\text{fus}}(P)/\text{K} = 0.326(11) P/\text{MPa} + 415.5(1.0) \quad (R^2 = 0.99) \quad (3)$$

195

196

197 4 DISCUSSION

198 4.1 COMPARISON OF THE STRUCTURE AND ITS THERMAL EXPANSION

199 The monoclinic structure, $P2_1/c$, of tetrazepam is characterized by dimers through C-H \cdots O (2.72 Å)
200 hydrogen bonds (see Figure 4 left-hand side). Similar dimers are present in related benzodiazepines such
201 as oxazepam, lorazepam, nitrozepam, and clonazepam (Neville et al., 1991, 1992). The stacking of the
202 dimers implies soft van der Waals interactions between them along the a axis (see Figure 4). Strong
203 intermolecular hydrogen bonds C-H \cdots O (2.46 and 2.54 Å) as well as C-H \cdots N (2.64 Å) are mainly present
204 along the bc plane (see Figure 4 left-hand side). The right-hand side of Figure 4 depicts the Hirshfeld
205 surface of the tetrazepam molecule in its crystal structure with the neighboring molecules and the
206 intermolecular interactions. Characteristic values of hydrogen bonds for tetrazepam at 150 K are given in
207 Table S6 of the Supplementary Materials. For comparison, the packing and the Hirshfeld surfaces of
208 diazepam and nordiazepam are provided in Figure S2 in the Supplementary Materials generated from the
209 structures reported in the literature at room temperature (Camerman and Camerman, 1972; D. Prasanna
210 and N. Guru Row, 2000; Dayananda et al., 2013). Table 1 compares the characteristic hydrogen bond
211 (inter and intramolecular) distances for tetrazepam as well as for diazepam and nordiazepam at room
212 temperature. From Table 1, it can be observed that tetrazepam is the only compound with intramolecular
213 C-H \cdots O hydrogen bonds, while comparable C-H \cdots N bonds, with quite similar characteristic distances are
214 present for all three compounds.

215 Figure 5 contains the 2D fingerprint plots of the O \cdots H and N \cdots H hydrogen bonds for tetrazepam,
216 diazepam, and nordiazepam. The intermolecular hydrogen bonds are quite similar and show up as spikes
217 (for short d_i and d_e distances) related to the donor atom (upper spike) and to the acceptor atom (lower
218 spike). As for tetrazepam, both short d_i and d_e distances are longer for the O \cdots H bonds than for the other
219 two compounds. On the other hand, the N \cdots H bonds of tetrazepam are shorter and the spikes in the
220 fingerprint plot are more localized, indicating strong interactions; these bonds are weaker for
221 nordiazepam and diazepam (see also Figure S2, Supplementary Materials). It is worth mentioning that for

222 nordiazepam, the shortest hydrogen bond is the N1-H11...O1 with a distance of only 2.03 Å as the
 223 fingerprint plot in Figure 5 top-right panel demonstrates; this is unmatched in the other compounds.

224 **Table 1. Characteristic intra- and intermolecular hydrogen bond distances in tetrazepam and**
 225 **related compounds diazepam and nordiazepam at room temperature**

Hydrogen Bonds	Intermolecular		Intramolecular	
	D-H...A	d(H...A) / Å	D-H...A	d(H...A) / Å
Tetrazepam	C2-H2B...O1	2.51	C16-H16A...N2	2.52
	C7-H7...O1	2.61	C16-H16A...O1	2.47
	C10-H10A...O1	2.75		
	C9-H8...N2	2.70		
Diazepam	C24-H24...O1	2.44		
	C22-H22...O1	2.53	C26-H26...N2	2.48
	C13-H13...N2	2.81		
	C15-H15...N2	2.79		
Nordiazepam	C15-H3...O1	2.65	C12-H2...N2	2.51
	N1-H11...O1	2.03		
	C3-H8...N1	2.79		
	C6-H10...N2	2.79		

226 The contributions of the relevant intermolecular contacts to the Hirshfeld surface areas are reported in
227 Figure 6 for tetrazepam and the related molecules diazepam and nordiazepam. It can be seen that the
228 relative contribution concerning the hydrogen bond O...H is smaller for the tetrazepam and higher for
229 nordiazepam, as the spikes of Figure 5 reveal. On the other hand, the contribution of the N...H is larger for
230 tetrazepam. The whole of the O...H, N...H and Cl...H contributions account for the 29.4, 26.6 and 28.4% for
231 tetrazepam, diazepam and nordiazepam, respectively, of the total surface contacts demonstrating the
232 relevance of the hydrogen bonds in all these structures.

233 In order to get an idea of the strength and the anisotropy of the intermolecular interactions of the
234 monoclinic phase of tetrazepam, the isobaric thermal expansion tensor (Salud et al., 1998) has been
235 determined. The deformation dU of a crystal due to a change of temperature dT is minimal in the
236 directions of the strongest intermolecular interactions and vice versa. Thus, the eigenvalues and
237 eigenvectors of the second-rank isobaric thermal expansion tensor α_{ij} , with $dU = \alpha_{ij}dT$, give insight into the
238 strength of the intermolecular interactions along three perpendicular directions in the crystal, commonly
239 referred to as “hard” and “soft” directions for strong and weak interactions respectively (Salud et al.,
240 1998).

241 The lattice parameters of tetrazepam were fitted as a function of the temperature using a standard least-
242 squares method for each parameter. Table S7 (Supplementary Materials) contains the refined lattice
243 parameters as well as the coefficients of the polynomial equations together with the reliability factor,
244 defined as $R = \sum \frac{(l_o - l_c)^2}{l_c^2}$, where l_o and l_c are the observed and calculated lattice parameters, respectively.

245 The program DEFORM (Filhol et al., 1987) was used for the calculation of the tensor. The same procedure
246 was followed for diazepam and nordiazepam. Powder X-ray diffraction patterns have been acquired as a
247 function of the temperature and the lattice parameters have been fitted using the published monoclinic
248 (P2₁/c) structures of diazepam (Dayananda et al., 2013) and nordiazepam (D. Prasanna and N. Guru Row,
249 2000).

250 For a monoclinic lattice, the tensor is completely defined by the principal coefficients, α_1 , α_2 , and α_3 , an
251 angle between the direction of one of the principal directions (α_3 , in the present case) and the
252 crystallographic axis \mathbf{a} , the α_2 eigenvector being parallel to the 2-fold axis \mathbf{b} of the monoclinic crystal. The
253 data can be found in Tables S8 and S9 in the Supplementary Materials.

254 Figure 7 represents the eigenvalues as a function of the temperature for the three compounds. In the case
255 of tetrazepam, the strongest intermolecular interactions reflected by negative tensor values indicating
256 contraction on heating (α_3 direction) can be found parallel to the bc plane and close to the c
257 crystallographic direction, while the soft direction (α_1) is rather close to the a direction, in perfect
258 agreement with the planes in which strong intermolecular hydrogen bonds appear. In diazepam, the soft
259 direction appears close to the two-fold axis b , while the strongest interactions are within the ac plane and
260 the hardest direction (α_3 eigenvector) is close to the crystallographic a direction related to strong
261 hydrogen bonds (see Figure S2 of the Supplementary Materials). In diazepam and nordiazepam, hard
262 directions result in only slightly negative eigenvalues (contraction) unlike tetrazepam for which
263 contraction exists in one direction along the whole temperature range from 100 K to the melting
264 temperature. Moreover, whereas tetrazepam and diazepam are entirely anisotropic in their thermal
265 expansion, the depiction of the thermal expansion tensor of nordiazepam resembles that of a donut, with a
266 slight contraction along the c direction and a virtually isotropic expansion in the two other directions.

267 4.2 STATISTICAL ANALYSIS OF THE SPECIFIC VOLUME OF TETRAZEPAM

268 The specific volume of tetrazepam as a function of the temperature is represented by eq. 2 and combines
269 data of both X-ray powder diffraction and single crystal X-ray diffraction at 150 and 293 K. The datapoints
270 are presented in Figure 1. Eq. 2 leads to the expansivity for tetrazepam of $\alpha_v = 2.03 \cdot 10^{-4} \text{ K}^{-1}$, i.e. close to
271 the mean value of $2.21 \cdot 10^{-4} \text{ K}^{-1}$ found for solids consisting of small organic molecules (Ceolin and
272 Rietveld, 2017; Céolin and Rietveld, 2015; Rietveld and Céolin, 2015). Nevertheless, the lattice expansion
273 is highly anisotropic; the asphericity index (Weigel et al., 1978) ranges between 0.52 at 150 K and 0.39 at
274 400 K. The anisotropy is similar to those of tienoxolol (Nicolai et al., 2013) and ascorbic acid (Nicolai et al.,
275 2017).

276 With eq. 2, the specific volume of crystalline tetrazepam at its temperature of fusion (i.e. its triple point of
277 415.6 K) is found to be $0.7774 \text{ cm}^3 \text{ g}^{-1}$, which becomes $0.777(2) \text{ cm}^3 \text{ g}^{-1}$ with the error taken into account.
278 From eq. 3, the slope of the solid-liquid equilibrium is found to be $dT/dP = 0.326(11) \text{ K MPa}^{-1}$. Using the
279 enthalpy of fusion, $\Delta_{\text{fus}}H = 88.6(4.6) \text{ J g}^{-1}$, and the melting point, $T_{\text{fus}} = 415.6(1.2) \text{ K}$, and inserting these into
280 the Clapeyron equation (eq. 1) one can calculate the volume change that accompanies the melting
281 transition $\Delta_{\text{fus}}V = v_L - v_S = 0.069 \text{ cm}^3 \text{ g}^{-1}$. Adding this value to the specific volume of the crystalline solid at

282 T_{fus} leads to the specific volume of the melt at this temperature. It results in $v_{L,\text{fus}}(T = 415.6 \text{ K}) = 0.847(5)$
 283 $\text{cm}^3 \text{g}^{-1}$ and the ratio v_L/v_S at T_{fus} equals therefore 1.089(6), i.e. close to the value of 1.11 ± 0.04 , previously
 284 found for a number of molecular compounds (Barrio et al., 2019; Ceolin and Rietveld, 2017; Céolin and
 285 Rietveld, 2015; Céolin and Rietveld, 2020; Rietveld and Céolin, 2015).

286 **Table 2. Ratio between the specific volumes of the liquid (v_L) and the solid (v_S) at the triple point**
 287 **($\approx T_{\text{fus}}$) and the volume change at the triple point ($\Delta v = v_L - v_S$). I or II following the compound name**
 288 **indicates the polymorph, X' being the metastable polymorph at normal pressure.**

	compound	T_{fus}/K	$v_L(T_{\text{fus}}) /$ $\text{cm}^3 \cdot \text{g}^{-1}$	$v_S(T_{\text{fus}})$ $/\text{cm}^3 \cdot \text{g}^{-1}$	v_L/v_S	$v_L - v_S$ $/\text{cm}^3 \cdot \text{g}^{-1}$	Reference
1	Paracetamol-I	442.3	0.9091	0.7935	1.14 ₅	0.1155	Espeau2005
1'	Paracetamol-II	430.2	0.9025	0.7679	1.17 ₅	0.1346	Espeau2005
2	Prilocaine	311.5	1.000	0.8840	1.13	0.1160	Rietveld2013
3	Rimonabant-I	428.3	0.8284	0.7554	1.11	0.0721	Perrin2013
3'	Rimonabant-II	429.2	0.8289	0.7480	1.11	0.080	Perrin2013
4	Biclotymol-I	400.5	0.9032	0.8000	1.13	0.1032	Ceolin2008
4'	Biclotymol-II	373.8	0.8813	0.8437	1.05	0.0394	Ceolin2008
5	Ternidazole	333.0	0.7989	0.6970	1.15	0.1019	Mahe2011
6	Morniflumate	348.1	0.8062	0.7192	1.12	0.0869	Barrio2017
7	Etifoxine	362.4	0.8599	0.78905	1.09	0.0709	Barrio2019
8	Progesterone-I	402.2	0.9590	0.8801	1.09	0.0789	Barrio2009
8'	Progesterone-II	394.5	0.9521	0.8788	1.08	0.0733	Barrio2009
9	Lidocaine	340.9	1.0337	0.9761	1.06	0.0576	Céolin2010

10	Tetrazepam	415.6	0.8469	0.7774	1.09	0.069	This work
----	------------	-------	--------	--------	------	-------	-----------

289 In 2004, Goodman et al. reported on the relationship between organic solid density ρ_s and liquid density
290 ρ_L at the melting triple point T_t (Goodman et al., 2004). In the article, the authors wrote that a “*a simple*
291 *ratio of the two densities $\rho_s(T_t)/\rho_L(T_t) = 1.17$ [T_t being the triple point temperature] was [previously] found*
292 *to be adequate and reliable for most organic compounds*”. They proposed to extend this ratio “*to include a*
293 *temperature dependence for solid density from T_t to substantially lower temperatures*” and they concluded
294 that “*the new correlation gives a ratio of solid to liquid density at the triple point of 1.12 instead of 1.17...*
295 *with an estimated average uncertainty of about 6%*” (i.e., 1,12(7)).

296 That the ratio of the two densities, i.e. the ratio of the two specific volumes, is constant is an implicit
297 ‘working’ assumption in Goodman’s paper, which should be questioned. The experimental values of v_L/v_S
298 at the melting triple point for a number of organic molecular compounds are compiled in Table 2. These
299 values have also been represented in Figure 8, together with the corresponding error bars. They have
300 been plotted against Δv to facilitate visualization of the variation in the ratios, because the key factors
301 affecting the v_L/v_S ratio are for now unknown.

302 5 CONCLUSIONS

303 The structure of tetrazepam has been determined at 150 K as monoclinic with space group $P2_1/c$, the
304 same as previously found at room temperature. The intermolecular interactions concern both intra and
305 intermolecular hydrogen bonds. Soft van der Waals interactions enable stacking of dimers along the a
306 crystallographic direction, whereas strong intermolecular hydrogen bonds are mainly located along the bc
307 monoclinic plane. The hydrogen bond network as well as the intermolecular contacts have been compared
308 through the Hirshfeld surface areas and fingerprint plots to those of the closely related molecules
309 diazepam and nordiazepam.

310 The analysis reveals that, whereas $N\cdots H$ intramolecular hydrogen bonds are present in all the studied
311 materials, intramolecular $O\cdots H$ hydrogen bonds only appear in the case of tetrazepam. As for the close
312 contacts, studied through the Hirshfeld surface analysis, the $O\cdots H$, $N\cdots H$, and $Cl\cdots H$ contributions with
313 respect the total surface contacts are quite similar for tetrazepam, diazepam and nordiazepam (29.4, 26.6
314 and 28.4% respectively).

315 Eigenvalues and the associated hard and soft directions of the thermal expansion tensor have been
316 determined for tetrazepam, diazepam and nordiazepam. They demonstrate noticeable differences
317 especially for the direction and intensity in which the respective lattices contract. Tetrazepam in
318 particular exhibits a contraction with increasing temperature over the entire monitored temperature
319 range approximately along the *c* crystallographic axis with a thermal expansion tensor value of about 10^{-3}
320 K^{-1} .

321 Finally, with the analysis of several active pharmaceutical ingredients, it has been demonstrated that the
322 ratio between the liquid and solid specific volumes at the melting point vary within a relatively limited
323 range. Although a greater number of pharmaceuticals must be studied, the trend clearly shows that this
324 ratio is not constant. This is important, because predicting the density of the liquid for pharmaceuticals
325 that can easily decompose in the liquid state (as many APIs do), will allow the calculation of the slope of
326 the solid-liquid equilibrium. This slope in turn will allow the construction of the so-called topological
327 pressure-temperature phase diagram with standard laboratory DSC and XRD data. Finally, the phase
328 diagram specifies the equilibrium conditions of the different polymorphs, which is important for the
329 formulation stage in drug development.

330 ACKNOWLEDGEMENTS

331 The authors are grateful for the financial support received within Projects No. FIS2017-82625-P from
332 MINECO and Project No. 2017SGR-042 from the Generalitat de Catalunya.

333 REFERENCES

- 334 Agilent-Technologies, 2014. CrysAlisPro, Version 1.171.37.35 (release 13-08-2014 CrysAlis171.NET) ed.
- 335 Allouchi, H., Ceolin, R., Gueiffier, A., Rietveld, I.B., 2019. A network of weak hydrogen bonds in the crystal
336 structure of Tetrazepam. *Ann Pharm Fr* 77, 121-125.
- 337 Allouchi, H., Nicolai, B., Barrio, M., Ceolin, R., Mahe, N., Tamarit, J.-L., Do, B., Rietveld, I.B., 2014. On the
338 Polymorphism of L-Citrulline: Crystal Structure and Characterization of the Orthorhombic delta Form.
339 *Cryst. Growth Des.* 14, 1279-1286.

340 Barrio, M., Allouchi, H., Tamarit, J.L., Ceolin, R., Berthon-Cedille, L., Rietveld, I.B., 2019. Experimental and
341 topological determination of the pressure-temperature phase diagram of racemic etifoxine, a
342 pharmaceutical ingredient with anxiolytic properties. *Int. J. Pharm.* 572, 118812.

343 Barrio, M., Maccaroni, E., Rietveld, I.B., Malpezzi, L., Masciocchi, N., Ceolin, R., Tamarit, J.L., 2012. Pressure-
344 temperature state diagram for the phase relationships between benfluorex hydrochloride forms I and II: a
345 case of enantiotropic behavior. *J. Pharm. Sci.* 101, 1073-1078.

346 Barrio, M., Tamarit, J.L., Ceolin, R., Robert, B., Guechot, C., Teulon, J.M., Rietveld, I.B., 2017. Experimental
347 and topological determination of the pressure temperature phase diagram of morniflumate, a
348 pharmaceutical ingredient with anti-inflammatory properties. *J. Chem. Thermodyn.* 112, 308-313.

349 Bauer, J., Spanton, S., Henry, R., Quick, J., Dziki, W., Porter, W., Morris, J., 2001. Ritonavir: An extraordinary
350 example of conformational polymorphism. *Pharm. Res.* 18, 859-866.

351 Brown, M.E., Glass, B.D., 2003. Decomposition of solids accompanied by melting - Bawn kinetics. *Int. J.*
352 *Pharm.* 254, 255-261.

353 Camerman, A., Camerman, N., 1972. Stereochemical basis of anticonvulsant drug action. II. Molecular
354 structure of diazepam. *J. Am. Chem. Soc.* 94, 268-272.

355 Ceolin, R., Rietveld, I.B., 2017. The topological phase diagram of cimetidine: A case of overall monotropy.
356 *Ann. Pharm. Fr.* 75, 89-94.

357 Céolin, R., Rietveld, I.B., 2015. The topological pressure-temperature phase diagram of ritonavir, an
358 extraordinary case of crystalline dimorphism. *Ann. Pharm. Fr.* 73, 22-30.

359 Céolin, R., Rietveld, I.B., 2020. Topological pressure-temperature state diagram of the crystalline
360 dimorphism of 2,4,6-trinitrotoluene. *Fluid Phase Equilib.* 506, 112395-112400.

361 Chaudhuri, K.R., 2008. Crystallisation within transdermal rotigotine patch: is there cause for concern?
362 *Expert Opin Drug Del* 5, 1169-1171.

363 Clark, R.C., Reid, J.S., 1995. Empirical absorption correction using spherical harmonics, implemented in
364 SCALE3 ABSPACK scaling algorithm. *Acta Crystallogr.* A51, 887-897.

365 D. Prasanna, M., N. Guru Row, T., 2000. Analysis of weak interactions involving fluorine: a comparative
366 study of crystal packing of some benzodiazepinone drug intermediates and their non-fluorinated
367 analogues. *CrystEngComm* 2, 134-140.

368 Dayananda, A.S., Yathirajan, H.S., Gerber, T., Hosten, E., Betz, R., 2013. Redetermination of the structure of
369 7-chloro-1,3-dihydro-1-methyl-5- phenyl-1,4-benzodiazepin-2(3H)-one, C₁₆H₁₃ClN₂O. Zeitschrift für
370 Kristallographie - New Crystal Structures 228, 223.

371 Farrugia, L.J., 2012. WinGX and ORTEP for Windows: an update. J. Appl. Crystallogr. 45, 849-854.

372 Filhol, A., Lajzerowicz, J., Thomas, M., 1987. DEFORM.

373 Goodman, B.T., Wilding, W.V., Oscarson, J.L., Rowley, R.L., 2004. A note on the relationship between
374 organic solid density and liquid density at the triple point. J. Chem. Eng. Data 49, 1512-1514.

375 Henriët, T., Gana, I., Ghaddar, C., Barrio, M., Cartigny, Y., Yagoubi, N., Do, B., Tamarit, J.-L., Rietveld, I.B.,
376 2016. Solid state stability and solubility of triethylenetetramine dihydrochloride. Int. J. Pharm. 511, 312-
377 321.

378 Huang, S., O'Donnell, Delpon de Vaux, S.M., O'Brien, J., Stutzman, J., Williams III, R.O., 2017. Processing
379 thermally labile drugs by hot-melt extrusion: The lesson with gliclazide. Eur. J. Pharm. Biopharm. 119, 56-
380 67.

381 Hubschle, C.B., Sheldrick, G.M., Dittrich, B., 2011. ShelXle: a Qt graphical user interface for SHELXL. J. Appl.
382 Crystallogr. 44, 1281-1284.

383 Ledru, J., Imrie, C.T., Pulham, C.R., Céolin, R., Hutchinson, J.M., 2007. High pressure differential scanning
384 Calorimetry investigations on the pressure dependence of the melting of paracetamol polymorphs I and II.
385 J. Pharm. Sci. 96, 2784-2794.

386 Macrae, C.F., Bruno, I.J., Chisholm, J.A., Edgington, P.R., McCabe, P., Pidcock, E., Rodriguez-Monge, L., Taylor,
387 R., Van De Streek, J., Wood, P.A., 2008. Mercury CSD 2.0- new features for the visualization and
388 investigation of crystal structures. J. Appl. Crystallogr. 41, 466-470.

389 Mahé, N., Nicolai, B., Allouchi, H., Barrio, M., Do, B., Céolin, R., Tamarit, J.-L., Rietveld, I.B., 2013. Crystal
390 Structure and Solid-State Properties of 3,4-Diaminopyridine Dihydrogen Phosphate and Their Comparison
391 with Other Diaminopyridine Salts. Cryst. Growth Des. 13, 708-715.

392 Neville, G.A., Beckstead, H.D., Shurvell, H.F., 1991. Fourier transform Raman and infrared study of
393 nitrazepam, nimetazepam, clonazepam and flunitrazepam. Vib. Spectrosc 1, 287-297.

394 Neville, G.A., Beckstead, H.D., Shurvell, H.F., 1992. An FT-Raman and IR study of oxaxepam, temazepam,
395 lorazepam, and Lormetazepam, Spectroscopicum Internationale. Colloquium (27 ; Bergen 1991-06-09).
396 Polyscience, Morin Heights, PQ, pp. 18-29.

397 Nicolai, B., Barrio, M., Tamarit, J.L., Ceolin, R., Rietveld, I.B., 2017. Thermal expansion of L-ascorbic acid.
398 Eur. Phys. J. - S.T. 226, 905-912.

399 Nicolai, B., Rietveld, I.B., Barrio, M., Mahé, N., Tamarit, J.-L., Céolin, R., Guéchet, C., Teulon, J.-M., 2013.
400 Uniaxial negative thermal expansion in crystals of tienoxolol. Struct. Chem. 24, 279-283.

401 Rietveld, I.B., Barrio, M., Lloveras, P., Ceolin, R., Tamarit, J.L., 2018. Polymorphism of spironolactone: An
402 unprecedented case of monotropy turning to enantiotropy with a huge difference in the melting
403 temperatures. Int. J. Pharm. 552, 193-205.

404 Rietveld, I.B., Ceolin, R., 2015. Rotigotine: Unexpected Polymorphism with Predictable Overall Monotropic
405 Behavior. J. Pharm. Sci. 104, 4117-4122.

406 Rietveld, I.B., Céolin, R., 2015. Phenomenology of crystalline polymorphism: overall monotropic behavior
407 of the cardiotoxic agent FK664 forms A and B. J. Therm. Anal. Calorim. 120, 1079-1087.

408 Rodriguez-Carvajal, J., 1993. Recent advances in magnetic structure determination by neutron powder
409 diffraction. Physica B 192, 55-69.

410 Rodriguez-Carvajal, J., Roisnel, T., Gonzales-Platas, J., 2005. Full-Prof suite version 2005, Laboratoire Léon
411 Brillouin, CEA-CNRS, CEN Saclay, France.

412 Salud, J., Barrio, M., Lopez, D.O., Tamarit, J.L., Alcobé, X., 1998. Anisotropy of intermolecular interactions
413 from the study of the thermal-expansion tensor. J. Appl. Crystallogr. 31, 748-757.

414 Sheldrick, G.M., 2008. A short history of SHELX. Acta Crystallogr. A 64, 112-122.

415 Tetko, I.V., Sushko, Y., Novotarskyi, S., Patiny, L., Kondratov, I., Petrenko, A.E., Charochkina, L., Asiri, A.M.,
416 2014. How accurately can we predict the melting points of drug-like compounds. J. Chem. Inf. Model. 54,
417 3320-3329.

418 Toscani, S., de Oliveira, P., Céolin, R., 2002. Phenomenology of polymorphism IV. The trimorphism of
419 ferrocene and the overall metastability of its triclinic phase. J. Solid State Chem. 164, 131-137.

420 Valentini, S., Romanini, M., Franco, L., Puiggali, J., Tamarit, J.L., Macovez, R., 2018. Tuning the kinetic
421 stability of the amorphous phase of the chloramphenicol antibiotic. Mol. Pharmaceut. 15, 5615-5624.

422 Weigel, D., Beguemi, T., Garnier, P., Berar, J.F., 1978. Evolution of thermal-expansion tensor as function of
423 temperature .1. General law of evolution of tensor symmetry. J. Solid State Chem. 23, 241-251.

424 Würflinger, A., 1975. Differential thermal-analysis under high-pressure IV. Low-temperature DTA of solid-
425 solid and solid-liquid transitions of several hydrocarbons up to 3 kbar. Ber. Bunsen-Ges. Phys. Chem. 79,
426 1195-1201.

427 **Figure Captions**

428 **Figure 1.** Specific volume of tetrazepam as a function of the temperature obtained from X-ray powder
429 diffraction (open circles) and from single crystal X-ray diffraction at 150 K and 293 K (filled circles). Inset:
430 tetrazepam molecular structure $C_{16}H_{17}ClN_2O$, $M = 288.77 \text{ g mol}^{-1}$.

431 **Figure 2.** Differential scanning calorimetry curves of racemic monoclinic tetrazepam obtained at 10 K
432 min^{-1} . Curve **(1)** first heating from room temperature of the crystalline monoclinic tetrazepam and curve
433 **(2)** second heating after quenching the melt at 200 K. Inset: enlargement of the glass transition event.

434 **Figure 3. (a)** Pressure-temperature phase diagram for the solid-liquid equilibrium and **(b)** melting peaks
435 of tetrazepam at various pressures. Solid and dashed lines in **(a)** correspond to the linear fit (eq. 3) and a
436 power law fit to demonstrate the level of curvature, respectively.

437 **Figure 4.** Left panel: Monoclinic structure of tetrazepam at 150 K (ab plane). C-H \cdots O and C-H \cdots N
438 intermolecular hydrogen bonds are shown by dashed red and blue lines, respectively. Intramolecular
439 hydrogen bonds are shown by dashed green lines. Right panel: Hirshfeld surface for tetrazepam with
440 neighboring molecules linked through close contacts.

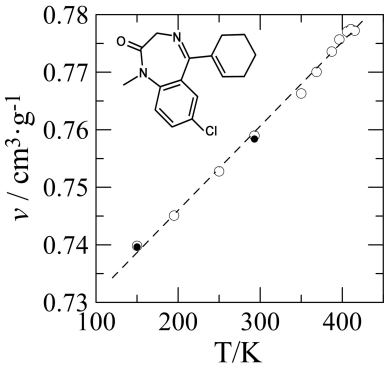
441 **Figure 5.** 2D fingerprint plots of tetrazepam (left), diazepam (center) and nordiazepam (right) for the
442 O \cdots H (top) and N \cdots H (bottom) close contacts at room temperature. The (d_i , d_e) frequency increases from
443 dark to light blue. The O \cdots H short contacts correspond to the N-H \cdots O (for example nordiazepam (2.03 Å),
444 see Table 1).

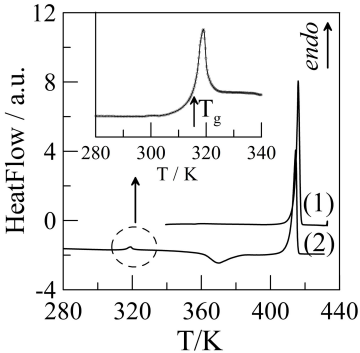
445 **Figure 6.** Comparison of the contributions (in percentage) to the Hirshfeld surface areas of a number of
446 intermolecular contacts: O \cdots H, N \cdots H, Cl \cdots H, H \cdots H and other minor contributions (C \cdots O, Cl \cdots O, C \cdots Cl,
447 Cl \cdots N, C \cdots C) for tetrazepam, diazepam, and nordiazepam.

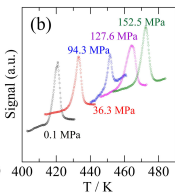
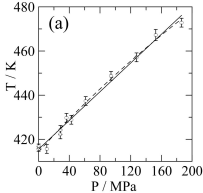
448 **Figure 7.** α_i eigenvalues of the thermal-expansion tensor as a function of temperature for tetrazepam
449 (top), diazepam (center), and nordiazepam (bottom). The α_2 eigenvector is parallel to the two-fold
450 crystallographic axis b . Right top insets correspond to the representation of the second-rank tensors (full
451 length scale of the α_i eigenvectors corresponds to 10^{-4} K^{-1}). Left top insets provide a schematic of the
452 molecule.

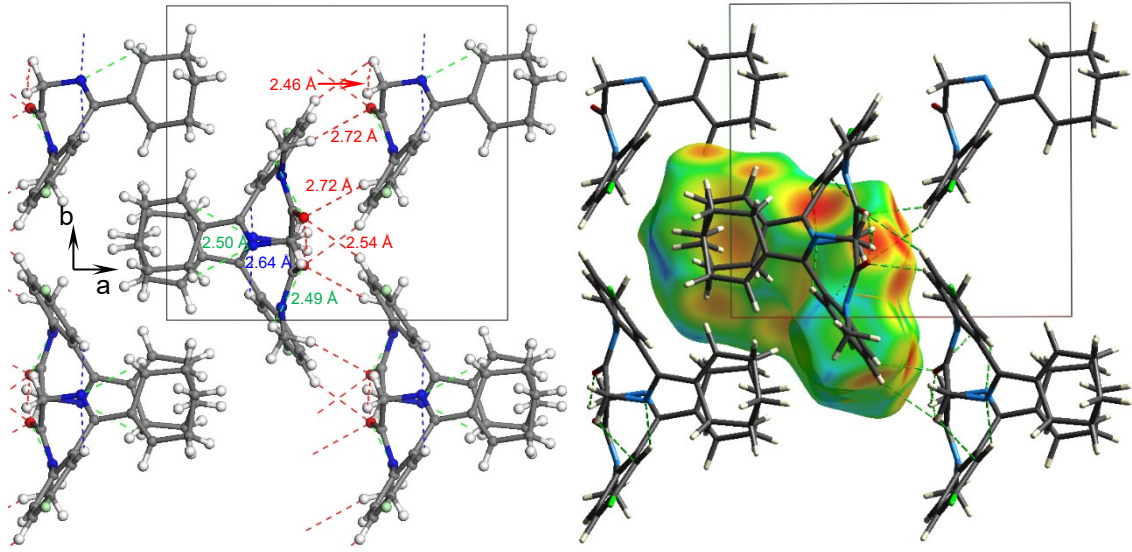
453 **Figure 8.** The ratio v_L/v_S at the melting triple point as a function of the volume change at the same
454 temperature. The numbers indicate the compound in Table 2. Grey circles correspond to the metastable
455 polymorphs at normal pressure as indicated in Table 2.

456

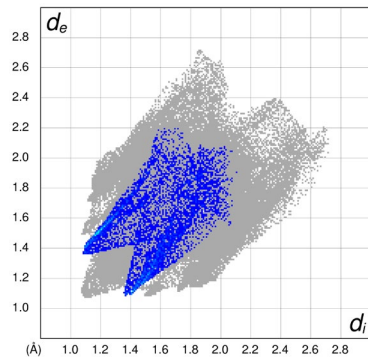




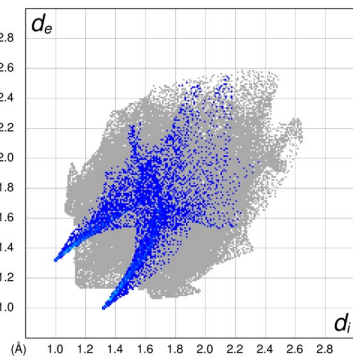




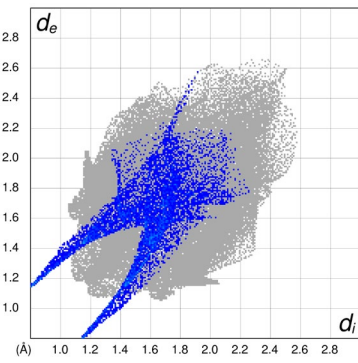
Tetrazepam O...H



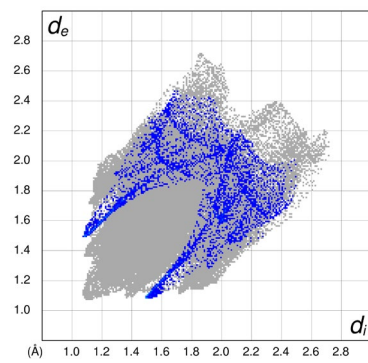
Diazepam O...H



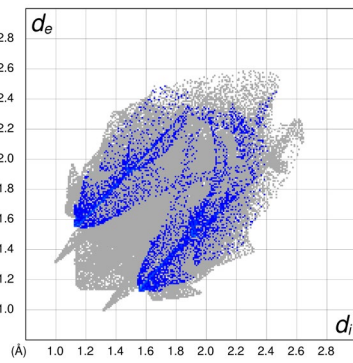
Nordiazepam O...H



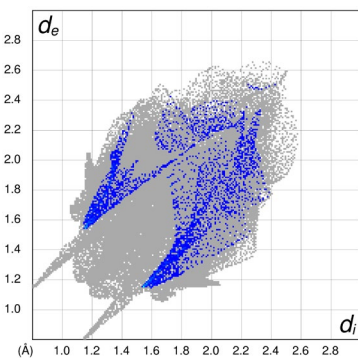
Tetrazepam N...H



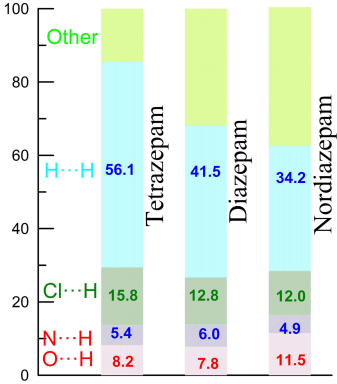
Diazepam N...H

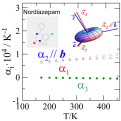
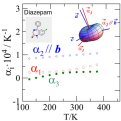
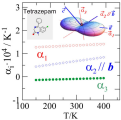


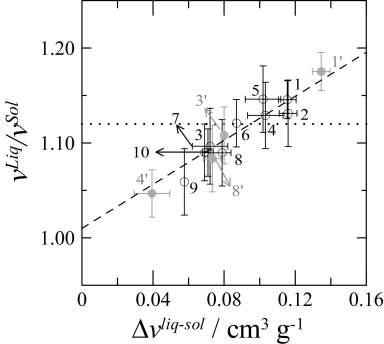
Nordiazepam N...H

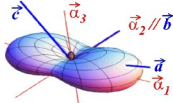
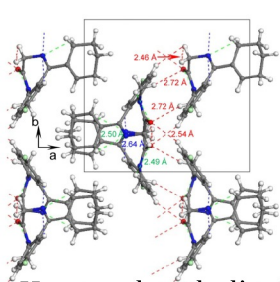


Percentage

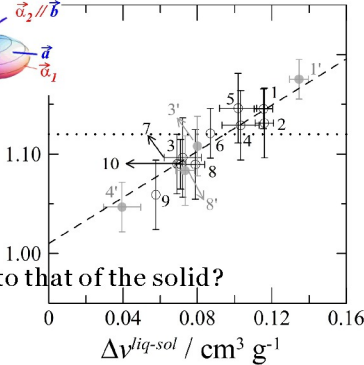








v^{Liq}/v^{Sol}



How to relate the liquid volume to that of the solid?